Deep-Water Carbonate Ion Concentrations in the Western Tropical Pacific Since the Mid-Pleistocene: A Major Perturbation During the Mid-Brunhes

B. Qin[1] (iD), T. Li[1,2,3] (iD), Z. Xiong[1,2] (iD), T. J. Algeo[4,5] (iD), and Q. Jia[1]

[1]Key Laboratory of Marine Sedimentology and Environmental Geology, First Institute of Oceanography, State Oceanic Administration, Qingdao, China, [2]Laboratory for Marine Geology, Qingdao National Laboratory for Marine Science and Technology, Qingdao, China, [3]College of Earth Sciences, University of Chinese Academy of Sciences, Beijing, China, [4]Department of Geology, University of Cincinnati, Cincinnati, OH, USA, [5]State Key Laboratories of Biogeology and Environmental Geology, Geological Processes and Mineral Resources, China University of Geosciences, Wuhan, China

Abstract We present a new deep-water carbonate ion concentration ([CO_3^{2-}]) record, reconstructed from the "size-normalized weight" of the planktonic foraminifer *Neogloboquadrina dutertrei* in core MD06-3047B, representing a middepth site (2.5 km) in the western tropical Pacific since 700 ka. On glacial-interglacial time scales, deep-water [CO_3^{2-}] exhibits an inverse relationship with global sea-level elevations, consistent with the "coral reef hypothesis" that the deep Pacific carbonate system responded to variations in shelf-carbonate production through the past 700 kyr. On longer time scales, a decoupling between deep-water [CO_3^{2-}] and $\delta^{13}C$ around the globe can be explained by a combination of continental weathering and nutrient inputs. During the mid-Brunhes interval (~600–200 ka), [CO_3^{2-}] reached a maximum of ~100 µmol kg^{-1} at the marine isotope stage (MIS) 12/11 boundary, followed by a steep decrease to a minimum of ~40 µmol kg^{-1} during middle MIS 11, representing the largest-amplitude change in [CO_3^{2-}] over the past 700 kyr. The [CO_3^{2-}] maximum records the largest deglacial oceanic carbon release since 700 ka, and the [CO_3^{2-}] minimum was a response to a global increase in pelagic carbonate production. From MIS 3 to 2 and from early to middle MIS 13, [CO_3^{2-}] showed rising trends opposite to those at water depths greater than 3.4 km, implying enhanced Pacific stratification during these intervals. These findings provide new insights into the Pleistocene evolution of the carbonate system in the Pacific Ocean.

Plain Language Summary The present study is significant in quantifying large-amplitude changes in deep Pacific [CO_3^{2-}] (from ~100 to 40 µ mol kg^{-1}) during the mid-Brunhes interval. We infer that the [CO_3^{2-}] maximum at the MIS 12/11 termination was the largest deglacial oceanic carbon release during the late Pleistocene, and that it may have contributed to the "mid-Brunhes climatic shift". The [CO_3^{2-}] minimum during the mid-MIS 11 corresponds to the well-known "mid-Brunhes dissolution interval," indicating a ~50% increase in pelagic carbonate production at that time. Moreover, the present study provides further evidence for the "coral reef hypothesis," that is, the deep Pacific carbonate system responded to variations in shelf-carbonate production on 100-kyr glacial-interglacial time scales.

1. Introduction

The Pleistocene evolution of the ocean's carbonate system has received much attention because changes in oceanic carbon inventories are considered to be potential primary drivers of past glacial-interglacial atmospheric CO_2 fluctuations (Broecker & Peng, 1987). Previous methods to investigate past changes in the Pacific carbonate system have made use mainly of foraminiferal $\delta^{13}C$ (Bickert et al., 1993; Mix et al., 1995a; Wang et al., 2004) and various qualitative carbonate dissolution proxies including sediment $CaCO_3$ content (Anderson et al., 2008; Farrell & Prell, 1989; Hodell et al., 2001), foraminiferal fragmentation (Le & Shackleton, 1992; Mix et al., 1995b; Zhang et al., 2007), and coarse fraction percent (Lalicata & Lea, 2011; Wu et al., 1990). Recently, benthic foraminiferal B/Ca (Kerr et al., 2017; Yu et al., 2013; Yu & Elderfield, 2007) and planktonic foraminiferal SNW (Broecker & Clark, 2001; Qin et al., 2017) have been developed as quantitative deep-water [CO_3^{2-}] proxies. These studies have improved our understanding of the Pacific carbon cycle.

Uncertainties remain regarding some aspects of the Pleistocene evolution of the Pacific carbonate system. For example, although most paleoceanographic records in the Pacific reveal that $CaCO_3$ abundance and

degree of carbonate preservation tend to have been higher during glaciations and lower during interglacials (i.e., "Pacific-type" carbonate stratigraphy), the cause of this pattern remains controversial. A number of studies have suggested that the Pacific carbonate system responds to sea-level-driven changes in shelf-carbonate production (Hodell et al., 2001; Kerr et al., 2017; Qin et al., 2017; Yu et al., 2013), whereas Sexton and Barker (2012) demonstrated that the Pacific pattern of $CaCO_3$ variation since 1 Ma was caused by strengthened ventilation within the Pacific sector of the Southern Ocean during glaciations. On longer time scales, 400- to 500-kyr periodicities are recognizable in Pleistocene marine $\delta^{13}C$ records from around the globe (Hoogakker et al., 2006), although the underlying forcings are still uncertain. Accurate reconstructions of deep-water $[CO_3^{2-}]$, which is intimately associated with pH and the concentration of dissolved CO_2 gas, can provide constraints necessary to evaluate the different mechanisms proposed for long-term $\delta^{13}C$ cycles. In addition to periodic changes, late Pleistocene evolution of the oceanic carbonate system is also characterized by a global carbonate dissolution centered around MIS 11 (the so-called "mid-Brunhes dissolution interval"; MBDI). This carbonate dissolution event has been widely recorded in many proxies from the global ocean (see Barker et al., 2006 for summary). However, the decline in deep-water $[CO_3^{2-}]$ and/or carbonate preservation extent during the MBDI cannot be quantified by traditional proxies. Benthic foraminiferal B/Ca can be used for deep-water $[CO_3^{2-}]$ reconstruction (Yu & Elderfield, 2007), but the B/Ca-based $[CO_3^{2-}]$ records cover the MBDI are currently scarce (Kerr et al., 2017; Sosdian et al., 2018). Continued application of paleo-$[CO_3^{2-}]$ proxies is essential for improving our understanding of the MBDI event and its relationship to contemporaneous climatic changes.

The SNW method was proposed by Lohmann (1995) and was further developed by Broecker and Clark (2001) and Qin et al. (2017) as a proxy for deep-water $[CO_3^{2-}]$ in the Pacific Ocean. Lohmann (1995) showed that the weight of whole foraminiferal shells picked from a narrow size range provides a measure of the extent of carbonate dissolution. Later, Broecker and Clark (2001) confirmed Lohmann's (1995) relationship between foraminiferal shell weight loss and lower deep-water $[CO_3^{2-}]$. Recently, Qin et al. (2017) evaluated the methodological assumptions behind the SNW proxy and suggested that the SNW of *Neogloboquadrina dutertrei* can be used to reconstruct past deep Pacific $[CO_3^{2-}]$. In this study, we present a new deep-water $[CO_3^{2-}]$ record based on the SNW of the planktonic foraminifer *N. dutertrei* for core MD06-3047B from the western tropical Pacific since 700 ka. The goals of this study are (1) to describe glacial-interglacial changes in deep Pacific $[CO_3^{2-}]$ since the mid-Pleistocene, (2) to discuss possible mechanisms for long-term cycles in marine $\delta^{13}C$ records by combining deep-water $[CO_3^{2-}]$ and $\delta^{13}C$ records from the global ocean, and (3) to identify and discuss the unusually large changes in deep-water $[CO_3^{2-}]$ during the MBDI.

2. Materials and Methods

Calypso Square core MD06-3047B was retrieved in the western tropical Pacific during the Marco Polo 2 cruise of the R/V Marion Dufresne in 2006. Core MD06-3047B is located at 17°N and 125°E in 2,510-m water depth (Figure 1). Deep-water $[CO_3^{2-}]$ is quite stable in the modern western tropical Pacific. The location of MD06-3047B is hardly influenced by North Pacific Deep Water, which is located at ~2-km water depth in the North Pacific and has an extremely low $[CO_3^{2-}]$ value (Figure 1). Therefore, site MD06-3047B is an ideal location for investigating past changes in deep-water $[CO_3^{2-}]$ in the western tropical Pacific.

The age model of the 890-cm-long core MD06-3047B, developed by Jia et al. (2018), is based on correlation of its benthic foraminifer *Cibicidoides wuellerstorfi* $\delta^{18}O$ profile with the standard LR04 curve (Lisiecki & Raymo, 2005), with additional refinement based on the last appearance datum of *Globigerinoides ruber* (pink). This age model shows that core MD06-3047B spans MIS 1 to 17, with the oldest recovered sediment layers dating to ~700 ka (Figure 2).

Whole shells of the planktonic foraminifer *N. dutertrei* in the 355- to 400-μm size range were selected at a sampling interval of 4 cm in core MD06-3047B and sorted into groups of ~50 shells. Each sample group was then subjected to a four-second sonication step in 2% sodium hexametaphosphate solution, following the protocol of Qin et al. (2016). Any shells broken during the cleaning process were discarded, and the remaining shells were counted. Note that breakage of thin-walled shells during the sonication cleaning step cannot be completely avoided, but this method provides a superior detritus cleaning effect with minimal shell
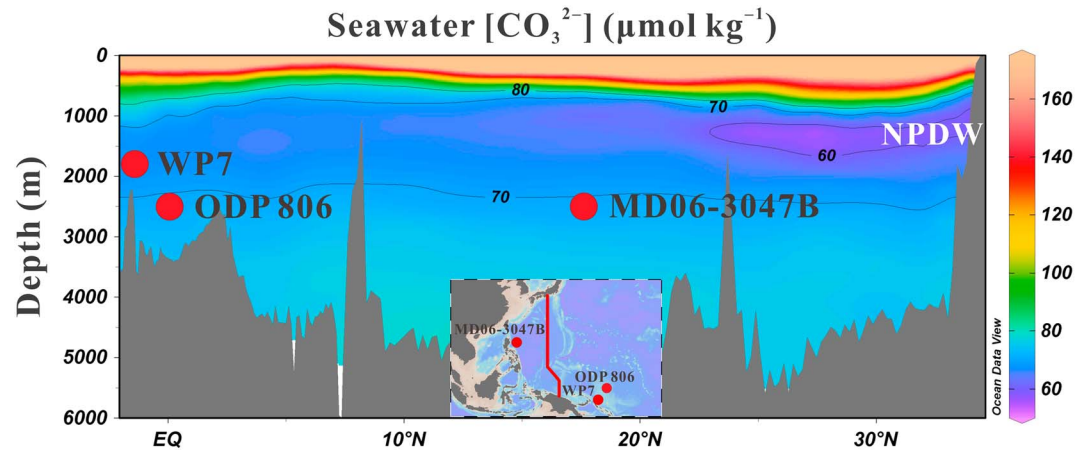
Figure 1. Location of study core MD06-3047B in the context of modern seawater $[CO_3^{2-}]$ estimated from the GLODAP data set (Key et al., 2004). The core WP7 (Qin et al., 2017) and ODP 806 (Kerr et al., 2017) were used for comparison, and the location of the meridional bathymetric profile of $[CO_3^{2-}]$ in the western Pacific (red line) is shown in the inset map. NPDW is North Pacific Deep Water.

breakage (Qin et al., 2016). All shells from each group were weighed together using a Sartorius CT2 P microbalance (precision <1 μg). Finally, shell diameters were measured using images taken at a known magnification with a LEICA MZ16 microscope and integrated camera system (Leica Application Suite V3.3.0).

The SNW for each sample was calculated by normalizing shell weight to the corresponding standard diameter:

$$SNW = \frac{W}{\sum_{i=1}^{n} D_i} \times D_{standard}$$

where W is the total shell weight for a single sample, D_i is the diameter of each individual shell in this sample, and $D_{standard}$ is the mean shell diameter of *N. dutertrei* in all samples from core MD06-3047B. *N. dutertrei* SNW

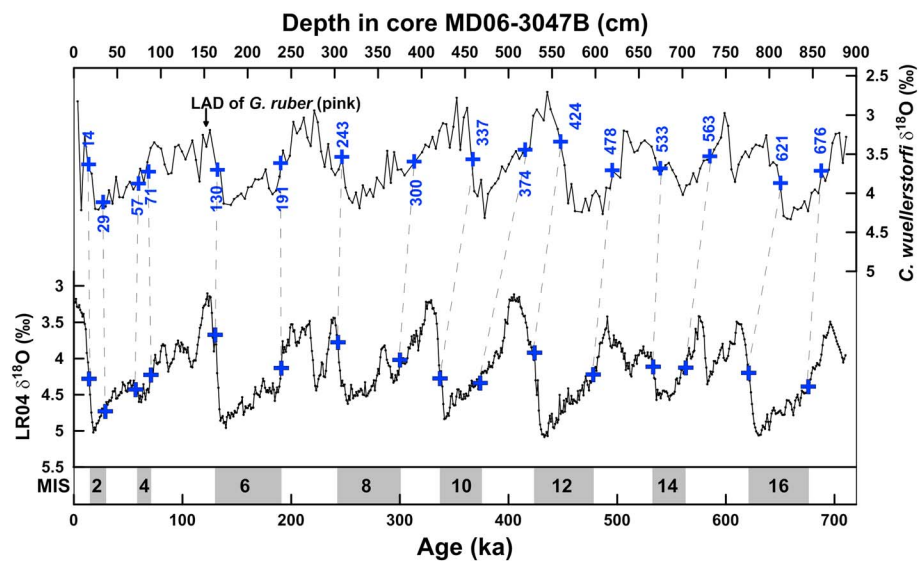**Figure 2.** Age model of MD06-3047B (Jia et al., 2018), obtained by comparing the *Cibicidoides wuellerstorfi* δ^{18}O curve and the standard LR04 stack (Lisiecki & Raymo, 2005), with additional refinement based on the last appearance datum (LAD) of *Globigerinoides ruber* (pink). The blue crosses represent oxygen-isotope events, and the black arrow indicates the LAD of *G. ruber* (pink).
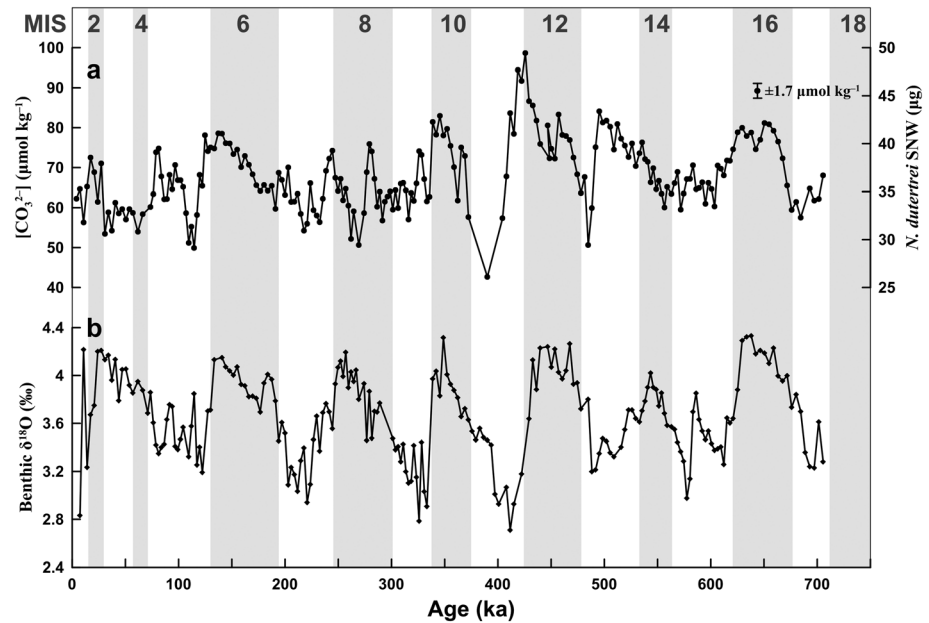
Figure 3. (a) Deep-water [CO_3^{2-}] based on the SNW of planktonic foraminifer *Neogloboquadrina dutertrei* for core MD06-3047B from the western tropical Pacific since 700 ka. Average error bar is indicated. (b) *Cibicidoides wuellerstorfi* $\delta^{18}O$ at site MD06-3047B (Jia et al., 2018).

were converted to deep-water carbonate saturation levels ($\Delta[CO_3^{2-}]$) based on a modern SNW-$\Delta[CO_3^{2-}]$ calibration for this species (Qin et al., 2017):

$$\Delta[CO_3^{2-}] = 2.4 \times SNW_{N.dutertrei} - 89.7 \ (R = +0.91)$$

Considering the negligible influence of glacial-interglacial changes in deep-water temperature, salinity, and pressure on calcite saturation concentration ([CO_3^{2-}]$_{sat}$) (Yu & Elderfield, 2007), preindustrial [CO_3^{2-}]$_{sat}$ can be used to reconstruct secular variation in [CO_3^{2-}] as follows:

$$[CO_3^{2-}] = \Delta[CO_3^{2-}] + [CO_3^{2-}]_{sat}$$

Preindustrial deep-water [CO_3^{2-}]$_{sat}$ values at site MD06-3047B were calculated using CO$_2$sys.xls (Pelletier et al., 2007), with K_1 and K_2 values from Mehrbach (1973) and KSO$_4$ values from Dickson (1990). CO$_2$sys.xls was run with preindustrial total dissolved inorganic carbon (DIC) from nearby GLODAP site 26677 (16.5°N, 124.5°E; Key et al., 2004), total alkalinity (ALK), deep-water temperature, salinity, and nutrient levels (PO$_4$ and SiO$_3$) from nearby World Ocean Atlas 2013 site 26601 (16.5°N, 124.5°E; Levitus et al., 2013). From this calculation, preindustrial deep-water [CO_3^{2-}]$_{sat}$ was ~70 μmol kg^{-1} at site MD06-3047B. Reproducibility of *N. dutertrei* SNW was determined by Qin et al. (2017) to yield a precision of ±0.7 μg (s.d.), corresponding to an error of ±1.7 μmol kg^{-1} in [CO_3^{2-}].

3. Results

Deep-water [CO_3^{2-}] estimated from *N. dutertrei* SNWs have ranged from 42.7 to 98.7 μmol kg^{-1} since 700 ka, with an average of 68.0 μmol kg^{-1} (Figure 3a). The [CO_3^{2-}] record exhibits a pattern of secular variation linked to ~100-kyr glacial-interglacial cycles; that is, [CO_3^{2-}] is generally higher during glacial stages and lower during interglacial stages. One obvious exception is seen during early to mid-MIS 13 (533–478 ka), where [CO_3^{2-}] shows an increase from ~70 to 80 μmol kg^{-1} (note: All MIS ages are from Lisiecki and Raymo, 2005). The [CO_3^{2-}] reached to a maximum of 98.7 μmol kg^{-1} at the MIS 12/11 boundary (at ~424 ka), followed by a steep decrease to a minimum of 42.7 μmol kg^{-1} at ~400 ka, representing the largest-amplitude change in [CO_3^{2-}] over the past 700 kyr.
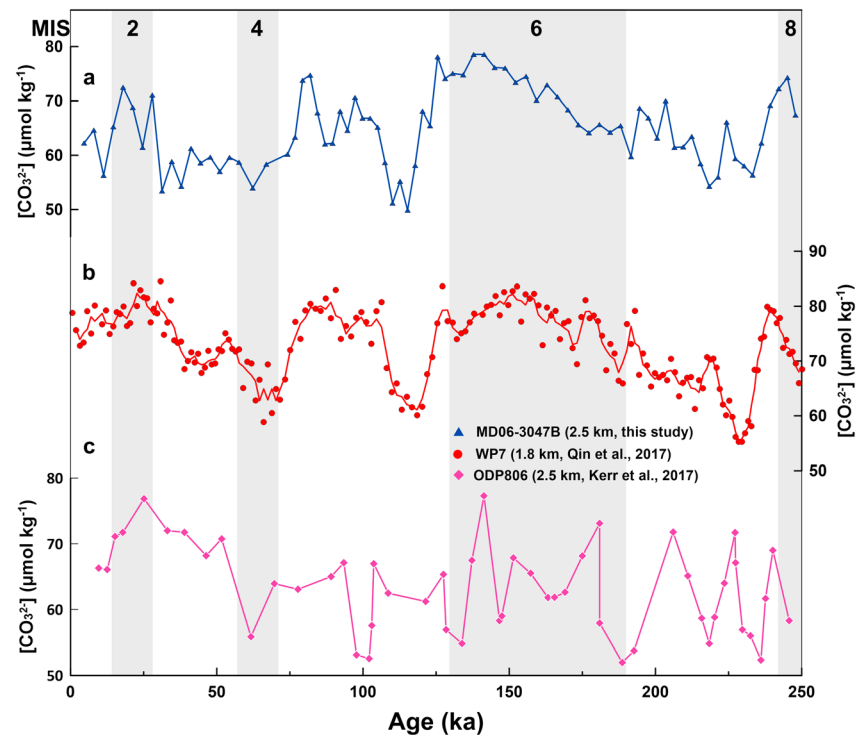
Figure 4. Deep-water [CO_3^{2-}] at (a) site MD06-3047B compared with deep-water [CO_3^{2-}] at (b) site WP7 (Qin et al., 2017) and (c) site ODP 806 (Kerr et al., 2017) since 250 ka. [CO_3^{2-}] was calculated from the SNW of *Neogloboquadrina dutertrei* in Figures 4a and 4b and from B/Ca of *Cibicidoides wuellerstorfi* in Figure 4c.

4. Discussion

4.1. Reliability of SNW Proxy

The SNW proxy can been applied to infer past deep-water [CO_3^{2-}] based on two key assumptions: (1) constancy through time of the offset between the [CO_3^{2-}] values of deep waters and pore waters (i.e., $\Delta[CO_3^{2-}]_{DW-PW}$) and (2) independence of the initial SNW from growth conditions, particularly surface-water [CO_3^{2-}]. Qin et al. (2017) assessed the validity of these two assumptions for *N. dutertrei* SNW in the western tropical Pacific and inferred that (1) respiration-driven dissolution, which can influence $\Delta[CO_3^{2-}]_{DW-PW}$, is limited owing to low productivity and high sediment $CaCO_3$ content and (2) the consistency between *N. dutertrei* SNW and other foraminiferal dissolution records indicates that the former is not manifestly biased by initial shell weight variation. The second assumption is at odds with previous studies that have shown planktic foraminiferal shell weights at sites in the Southern, Indian, and Atlantic Oceans to vary in response to changes in atmospheric pCO$_2$ (Barker & Elderfield, 2002; Moy et al., 2009; Naik et al., 2010). This phenomenon has been attributed to control of initial shell weights by surface-water [CO_3^{2-}], which is related to atmospheric pCO$_2$. This discrepancy between our study and previous studies stems from the fact that the deep-water carbonate saturation state in the Pacific Ocean is much lower than in other modern oceans (Key et al., 2004). That is, the effect of initial SNW variations is minor relative to the overwhelming control of carbonate dissolution on SNW in the Pacific Ocean (Qin et al., 2017). Therefore, the SNW of *N. dutertrei* can be used to reconstruct past deep Pacific [CO_3^{2-}].

The reliability of using *N. dutertrei* SNW as a proxy for deep-water [CO_3^{2-}] is further confirmed by comparison of our results for MD06-3047B with the [CO_3^{2-}] record of the WP7 core (Figures 4a and 4b). Cores MD06-3047B and WP7 are located on the northern margin and in the center of the Western Pacific Warm Pool, respectively. Today, although the ~3-μmol kg^{-1} difference in deep-water [CO_3^{2-}] between these two sites is negligible, the differences in upper-ocean hydrography are quite large (Key et al., 2004; Levitus et al., 2013). For example, at the mean calcification depth of *N. dutertrei* (~140 m; Rippert et al., 2016), the differences in temperature, salinity, and [CO_3^{2-}] between sites MD06-3047B and WP7 are −1.3 °C, −0.4‰, and

-26 μmol kg^{-1}, respectively. Moreover, it seems unlikely that upper-ocean hydrographic conditions at these two sites were exactly the same in the past. For example, the planktonic foraminiferal δ^{13}C of core MD06-3047B, which was related to nutrient concentrations and thermocline depth (Jia et al., 2015), displays a substantially different pattern from that of core WP7 (Li et al., 2011) since 250 ka. Therefore, we conclude that past changes in $\Delta[CO_3^{2-}]_{DW-PW}$ and initial shell weight of *N. dutertrei*, both of which are controlled by upper-ocean hydrographic conditions (Archer et al., 1989; De Villiers, 2004), should be different at sites MD06-3047B and WP7. However, the $[CO_3^{2-}]$ profile of core MD06-3047B exhibits a pattern of secular variation almost the same as that of core WP7 since 250 ka (Figures 4a and 4b), thus suggesting that the SNW-based $[CO_3^{2-}]$ records are not biased by $\Delta[CO_3^{2-}]_{DW-PW}$ and initial shell weight variations.

Today, deep Pacific carbonate dissolution is strong enough to overwhelm the $\Delta[CO_3^{2-}]_{DW-PW}$ and initial SNW signals. However, deep Pacific $[CO_3^{2-}]$ was higher during glacials than interglacials (Kerr et al., 2017; Qin et al., 2017; Yu et al., 2013). Therefore, $\Delta[CO_3^{2-}]_{DW-PW}$ and initial SNW signals may have been preserved under glacial conditions of weak carbonate dissolution, potentially biasing SNW-based $[CO_3^{2-}]$ reconstructions. For example, it has been suggested that initial SNW was relatively heavier during glacial stages than interglacials, due to a glacial decrease in atmospheric pCO$_2$ and a corresponding increase in surface-water $[CO_3^{2-}]$ (Barker & Elderfield, 2002). It is possible that this initial SNW signal was not completely erased at the seafloor owing to weak carbonate dissolution during glacial stages, producing a bias toward high values in the amplitude of glacial-interglacial variability in SNW-based $[CO_3^{2-}]$. For the purpose of testing this bias, we compared the SNW-based $[CO_3^{2-}]$ results (Figures 4a and 4b) with the B/Ca-based $[CO_3^{2-}]$ record at the nearby site ODP 806 (Kerr et al., 2017) since 250 ka (Figure 4c). The SNW-based $[CO_3^{2-}]$ profiles (Figures 4a and 4b) exhibit a pattern of secular variation broadly similar to the B/Ca-based $[CO_3^{2-}]$ record (Figure 4c). The overall lack of detailed correspondence between SNW-based and B/Ca-based $[CO_3^{2-}]$ records is likely due to the different sampling resolutions of these records. During the last two glacial-interglacial cycles, SNW-based $[CO_3^{2-}]$ have ranged from 51.2 to 78.6 μmol kg^{-1} at site MD06-3047B, and from 55.3 to 83.7 μmol kg^{-1} at site WP7 (Figures 4a and 4b). Similarly, B/Ca-based $[CO_3^{2-}]$ data cover a range of 52.0 to 77.3 μmol kg^{-1} at site ODP 806. Therefore, the amplitudes of glacial-interglacial variability in SNW-based $[CO_3^{2-}]$ are generally consistent with the B/Ca-based $[CO_3^{2-}]$ data. This consistency confirms the reliability of the SNW proxy even under conditions of weak carbonate dissolution.

4.2. Causes of $[CO_3^{2-}]$ Variation During Glacial-Interglacial Cycles

The consistency of reconstructed deep-water $[CO_3^{2-}]$ in cores MD06-3047B (this study) and WP7 (Qin et al., 2017) since 250 ka implies that the full 700-kyr $[CO_3^{2-}]$ profile of core MD06-3047B represents a robust record of temporal variability in the carbonate saturation state of the western tropical Pacific (Figure 5a). Recently, Kerr et al. (2017) generated a 500-kyr deep-water $[CO_3^{2-}]$ reconstruction from the western tropical Pacific using the B/Ca of the benthic foraminifer *C. wuellerstorfi* from site ODP 806 at 2,500-m water depth (Figure 5b). Deep Pacific $[CO_3^{2-}]$ records at sites MD06-3047B and ODP 806 reveal the same pattern on glacial-interglacial time scales, although there are differences between these two data sets during certain transient intervals (Figures 5a and 5b). Both our and Kerr et al. (2017)'s $[CO_3^{2-}]$ data display a so-called "Pacific-type" carbonate stratigraphy (Hodell et al., 2001; Figure 5c) characterized by generally high values (i.e., enhanced preservation) during glacial stages and low values (i.e., enhanced dissolution) during interglacials. The agreement between deep Pacific $[CO_3^{2-}]$ and carbonate content provides evidence to support previous suggestions (e.g., Anderson et al., 2008; Berger, 1973; Farrell & Prell, 1989; Hodell et al., 2001; Lalicata & Lea, 2011; Zhang et al., 2007) that ocean chemistry ($[CO_3^{2-}]$) is the principal factor controlling the content and accumulation rate of CaCO$_3$ in Pacific sediments. The key question thus becomes, what controlled glacial-interglacial changes in deep Pacific $[CO_3^{2-}]$?

Recent studies (Kerr et al., 2017; Qin et al., 2017; Yu et al., 2013) inferred that the ~100-kyr glacial-interglacial carbonate cycle in the deep Pacific was driven by changes in shelf-carbonate production (i.e., the "coral reef hypothesis"; Berger, 1982) based on negative correlations between deep-water $[CO_3^{2-}]$ and eustatic (global sea level) elevations since 500 ka. The results of the present study provide support for this hypothesis in that increases (decreases) in deep-water $[CO_3^{2-}]$ at MD06-3047B have coincided with decreases (increases) in eustatic elevations on glacial-interglacial time scales since 700 ka (Figures 5a and 5d). According to the coral reef hypothesis, coral growth rates were lower during glacial stages, when sea-level fall exposed continental
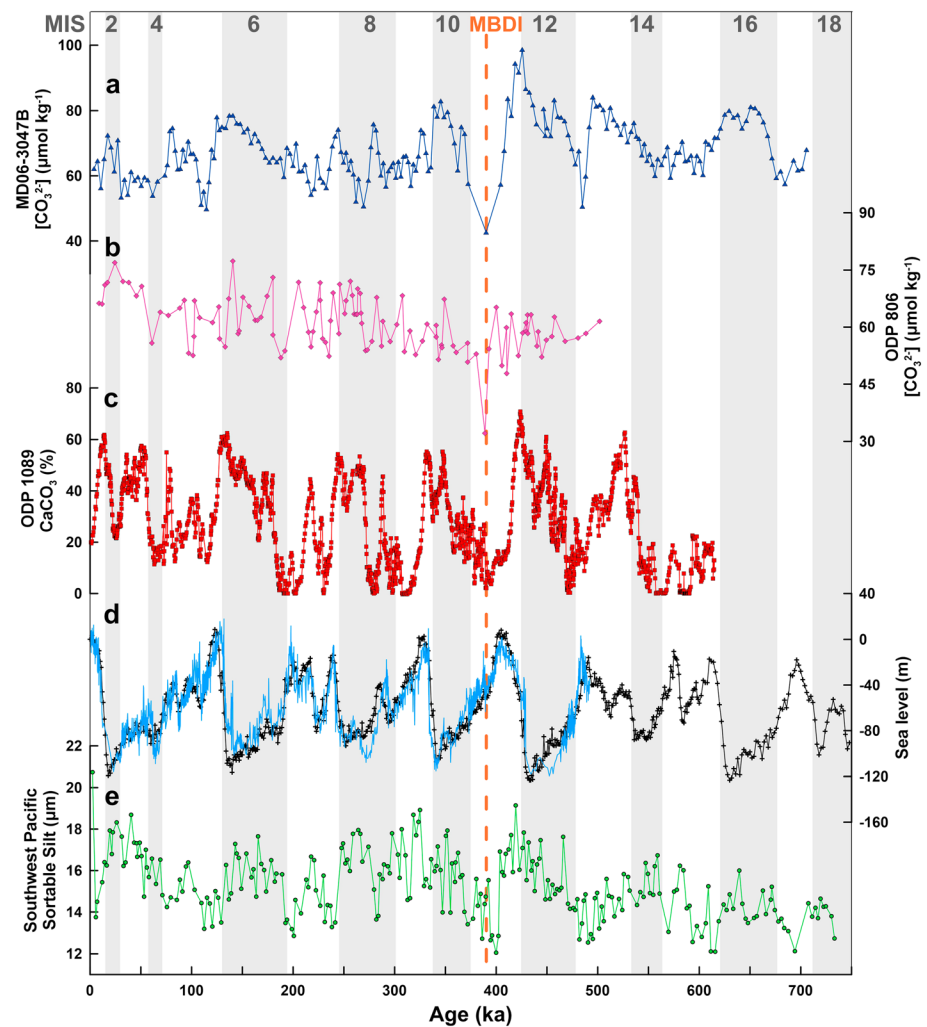
Figure 5. Deep-water $[CO_3^{2-}]$ at (a) site MD06-3047B (this study) compared with deep-water $[CO_3^{2-}]$ at nearby (b) site ODP 806 (Kerr et al., 2017), Pacific-pattern of deep-sea sedimentary calcium carbonate content change at (c) site ODP 1089 (note that although ODP1089 is from a site in the South Atlantic, it is bathed in Indo-Pacific deep water rather than by North Atlantic Deep Water; Hodell et al., 2001), (d) global sea-level elevation (Grant et al., 2014; Miller et al., 2011), and (e) Circumpolar Deep Water flow into the Pacific Ocean, as proxied by mean sortable silt size at ODP site 1123 east of New Zealand (Hall et al., 2001). The dashed line indicates the mid-Brunhes dissolution interval.

shelves. Reduction of shallow-water $CaCO_3$ burial implies a greater burial load for the deep sea, thereby triggering increases of deep-ocean $[CO_3^{2-}]$ by the mechanism of $CaCO_3$ compensation. Berger (1982) predicted that changes in deep-water $[CO_3^{2-}]$ should lag those in eustatic elevations by several thousand years. Although the temporal resolution of our data is too low to discuss the phase relationship between deep-water $[CO_3^{2-}]$ and eustasy, previous high-resolution research on sediment $CaCO_3$(Hodell et al., 2001) content and deep-water $[CO_3^{2-}]$ (Qin et al., 2017) confirmed an ~8-kyr lag of carbonate system response relative to sea-level changes.

Apart from the coral reef hypothesis, several other hypotheses have been advanced to account for glacial-interglacial changes in deep-water $[CO_3^{2-}]$. In the "rain ratio hypothesis" (Archer & Maier-Reimer, 1994), a glacial increase in deep-water $[CO_3^{2-}]$ is caused by an increase in the burial ratio of particulate organic carbon to calcium carbonate (POC:$CaCO_3$). This hypothesis, however, is not supported by the sediment $CaCO_3$ content or primary productivity records in the Pacific (see Qin et al., 2017, and references therein). In the "glacial Pacific ventilation hypothesis" (Sexton & Barker, 2012), a glacial increase in Pacific $[CO_3^{2-}]$ is explained by increased ventilation within the Pacific sector of the Southern Ocean. Based on

sedimentological (e.g., sortable silt, a proxy for Circumpolar Deep Water [CDW] inflow) and isotopic (e.g., benthic δ^{13}C difference between two sites, a proxy for deep-ocean ventilation) evidence from the South Pacific, Sexton and Barker (2012) inferred that strengthening of deep-water ventilation within the Pacific sector of the Southern Ocean by intensified CDW inflow reduced Pacific carbonate dissolution during glaciations since ~1 Ma. Our results are consistent with a positive relationship between deep-water $[CO_3^{2-}]$ and increased deep-water ventilation/CDW inflow (Figures 5a and 5e).

Whether glacial strengthening of ventilation state within the Pacific sector of the Southern Ocean would result in increases in deep Pacific $[CO_3^{2-}]$ is unclear. According to the glacial Pacific ventilation scenario (Sexton & Barker, 2012), interglacial deep Pacific carbonate saturation state is relatively low because much of the North Atlantic Deep Water-associated storage of regenerated nutrients and respired CO_2 is in the Pacific, at the end of a long deep-ocean "conveyor." But during glacial stages, the deep Pacific was ventilated directly by Southern Ocean watermasses with relatively low regenerated nutrient and respired CO_2 concentrations, thus increasing deep Pacific $[CO_3^{2-}]$ relative to interglacials. Although a greater stratification in the Southern Ocean during glacial stages than interglacials would have caused an increase in deep-ocean carbon storage and a corresponding decrease in deep-water $[CO_3^{2-}]$ (Anderson et al., 2009; Sigman et al., 2010), the main respired CO_2 storage in the Southern Ocean appears to have been in the Atlantic sector, not the Pacific sector (McCave et al., 2008; Ninnemann & Charles, 2002). However, several other studies (Adkins, 2013; Ferrari et al., 2014) have suggested that glacially strengthened Southern Ocean ventilation would have hindered vertical mixing and isolated the deep ocean, leading to a slowly ventilated reservoir in which carbon was stored, thereby triggering decreases of deep-water $[CO_3^{2-}]$ and dissolution of $CaCO_3$. This inference is supported by evidence of stratification of the North Pacific during glaciations (Brunelle et al., 2007; Gebhardt et al., 2008; Haug et al., 1999; Jaccard et al., 2005). Clearly, further work is needed to better estimate the effect of glacial-interglacial Southern Ocean abyssal ventilation patterns on the deep Pacific carbon cycle. At present, the bulk of evidence favors the coral reef hypothesis as the main cause of glacial-interglacial variations in deep Pacific $[CO_3^{2-}]$.

4.3. Decoupling of Ocean δ^{13}C and $[CO_3^{2-}]$ in 400- to 500-Kyr Cycles

On time scales longer than ~100-kyr glacial-interglacial cycles, our deep-water $[CO_3^{2-}]$ record exhibits no clearly discernable long-term trends since 700 ka (Figure 6b). Over the same interval, stacked benthic foraminiferal δ^{13}C records from the global ocean show evidence of an ~400- to 500-kyr cycle superimposed on glacial-interglacial cycles (Hoogakker et al., 2006; Figure 6a). Note that the δ^{13}C of a foraminifera shell reflects the carbon isotopic composition of the DIC in seawater in which the shell calcified. Such 400- to 500-kyr periodicities are present in Plio-Pleistocene δ^{13}C records from every major ocean basin (e.g., Bickert et al., 1993; Chen et al., 1995; Keigwin & Boyle, 1985; Mix, Pisias, et al., 1995; Oppo et al., 1995; Wang et al., 2003, 2004). Potential drivers for this long-term cycle in global-ocean δ^{13}C include continental weathering (Tian et al., 2011; Wang et al., 2004), POC:$CaCO_3$ rain ratio (Hoogakker et al., 2006), coccolithophore blooms (Rickaby et al., 2007), a combination of rain ratio and total productivity (Russon et al., 2010), a combination of weathering and nutrient inputs (Ma et al., 2011), and a microbial carbon pump (Ma et al., 2017; Wang et al., 2014). Clarifying whether the long-term cycles observed in benthic foraminiferal δ^{13}C records exist in deep-water $[CO_3^{2-}]$ can provide constraints necessary for an evaluation of these different mechanisms.

The 400- to 500-kyr periodicity in benthic foraminiferal δ^{13}C does not exist in the 700-kyr-long MD06-3047B $[CO_3^{2-}]$ record (Figure 6b). To ascertain whether this absence is a local or global feature of deep-water dissolution records, we synthesize $[CO_3^{2-}]$ and other dissolution proxy records such as benthic B/Ca, foraminiferal fragmentation, $CaCO_3$ content, and coarse fraction percent from the Pacific Ocean (Anderson et al., 2008; Bordiga et al., 2013; Farrell & Prell, 1989; Kerr et al., 2017; Le & Shackleton, 1992; Mix et al., 1995b; Wu et al., 1990; Yasuda et al., 1993; Zhang et al., 2007), Indian Ocean (Bassinot et al., 1994; Chen & Farrell, 1991; Nath et al., 2013), Atlantic Ocean (Flores et al., 2003; Gröger et al., 2003; Henrich et al., 2002; Hodell et al., 2001; Lear et al., 2016; Prell, 1982; Sosdian et al., 2018), Southern Ocean (Rickaby et al., 2010), and South China Sea (Wang et al., 2004). This analysis shows that 400- to 500-kyr periodicities are not present in any of these records. We illustrate this absence in selected dissolution records, including the $[CO_3^{2-}]$ record of this study (Figure 6b), a benthic foraminiferal B/Ca record from the Southern Ocean (Rickaby et al., 2010; Figure 6c), and the typical patterns of $CaCO_3$ variation in the Pacific and Atlantic Oceans (Hodell et al., 2001; Figures 6d and
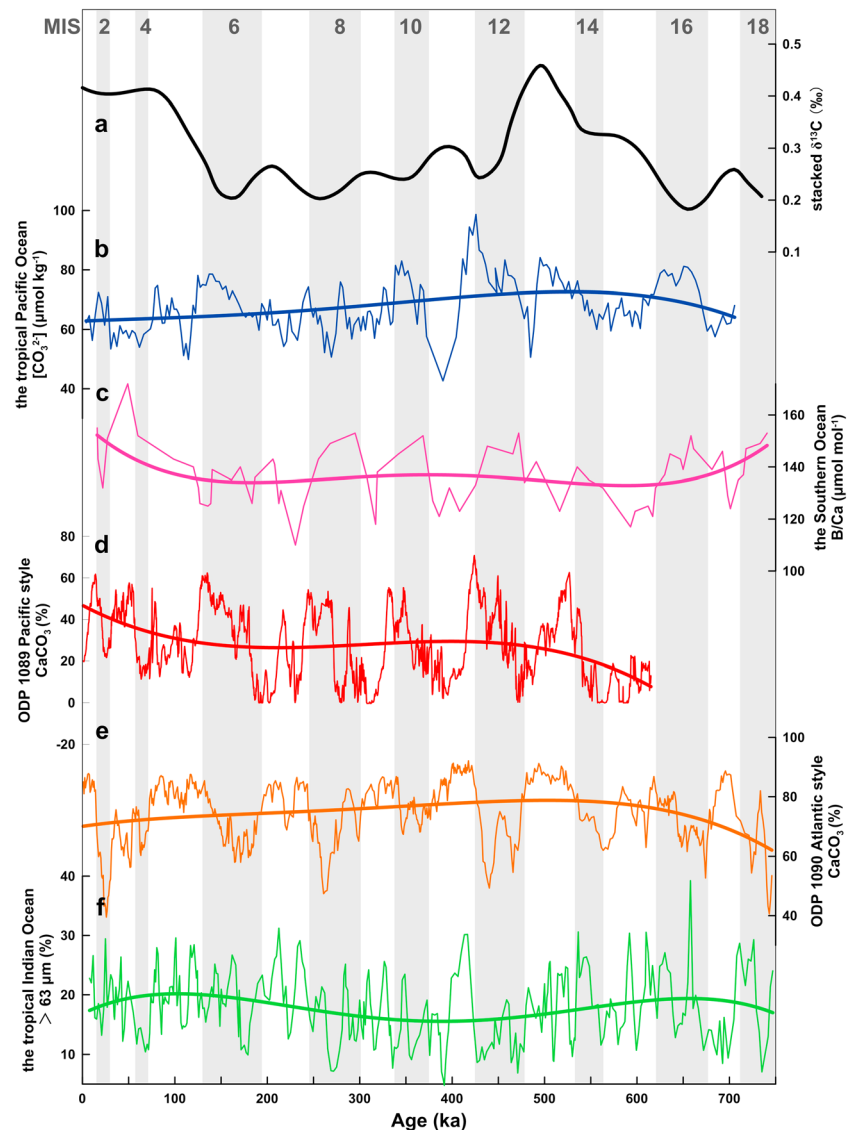
Figure 6. (a) Standardized mean or stacked benthic foraminiferal δ^{13}C record derived from benthic foraminiferal δ^{13}C data from the global ocean (Hoogakker et al., 2006). (b) Deep-water [CO_3^{2-}] in the western tropical Pacific (this study). (c) Benthic foraminiferal B/Ca in the Southern Ocean (Rickaby et al., 2010). (d and e) "Pacific-style" and "Atlantic-style" sedimentary $CaCO_3$ content cycles (Hodell et al., 2001). (f) Percentage of coarse fraction in the tropical Indian Ocean (Bassinot et al., 1994). The thick lines are polynomial fits shown to highlight general long-term trends in the original data sets. The ~400- to 500-kyr periodicity in (a) is not recognizable in (b)–(f).

6e). A ~400-kyr cycle has been observed in a coarse fraction percent record from the Indian Ocean (Bassinot et al., 1994; Figure 6f), but these variations are out-of-phase with the ~400- to 500-kyr δ^{13}C cycle (Figures 6a and 6f). Because the fine fraction of $CaCO_3$ is dominated by coccoliths and the coarse fraction by foraminifera (Chiu & Broecker, 2008; McCave et al., 1995), long-term increases (decreases) in the coarse fraction percent would result from increases (decreases) in initial foraminifer/coccolith ratios, reflecting declining (rising) coccolithophore production (Rickaby et al., 2007). We therefore speculate that the ~400-kyr cycle in Indian Ocean coarse fraction percent records (Bassinot et al., 1994; Chen & Farrell, 1991; Gröger et al., 2003; Prell, 1982) was related to variations in coccolithophore production rather than carbonate dissolution. In summary, we infer that global deep-ocean [CO_3^{2-}] and carbonate dissolution records do not contain evidence for the ~400- to 500-kyr cycles observed in benthic foraminiferal δ^{13}C records, at least during the last 700 kyr.

The MD06-3047B deep-water $[CO_3^{2-}]$ record, along with other $[CO_3^{2-}]$ and dissolution records discussed above, provides important tests of the various mechanisms proposed to account for long-term global-ocean $\delta^{13}C$ fluctuations during the late Quaternary. Several mechanisms, including hypotheses based on continental weathering, nutrient inputs, POC:CaCO$_3$ rain ratio, and carbon burial fluxes, call for synchronous fluctuations in deep-ocean $\delta^{13}C$ and $[CO_3^{2-}]$. Specifically, continental weathering of carbonate and silicate rocks leads to increases in ocean $[CO_3^{2-}]$ and carbonate preservation by adding DIC and alkalinity (ALK) to the global ocean (Hoogakker et al., 2006; Russon et al., 2010), triggering a net increase of burial of inorganic carbon ($\delta^{13}C \approx 0$ ‰) in relation to organic carbon ($\delta^{13}C \approx -25$‰) that will lead to a decrease in ocean $\delta^{13}C$ (Ma et al., 2011; Tian et al., 2011). On the other hand, enhanced nutrient inputs result in decreases in both $\delta^{13}C$ and $[CO_3^{2-}]$ due to increases in DIC/DOC ratios (n.b., DOC is dissolved organic carbon) and organic carbon remineralization (Hoogakker et al., 2006; Ma et al., 2017; Wang et al., 2014). In this scenario, a release of isotopically light carbon from the DOC pool to the DIC pool results in lighter DIC $\delta^{13}C$ (Ma et al., 2017; Wang et al., 2014), and an increase in CO$_2$ supply through release during organic carbon remineralization causes a decrease in deep-water $[CO_3^{2-}]$ (Hoogakker et al., 2006). In the POC:CaCO$_3$ rain ratio and/or carbon burial flux scenarios, increased organic carbon burial flux leads to an increase in $\delta^{13}C$ and a decrease in $[CO_3^{2-}]$ (Hoogakker et al., 2006; Rickaby et al., 2007; Russon et al., 2010). Therefore, there does not seem to be a single mechanism that can explain both the long-term cyclicity of $\delta^{13}C$ and the long-term stability of $[CO_3^{2-}]$. Moreover, the rain ratio mechanism was challenged by the discovery of the "ballast mineral" effect that CaCO$_3$ may be the most important agent for transporting organic carbon to the deep ocean (Armstrong et al., 2001; Klaas & Archer, 2002). If long-term cycles in $\delta^{13}C$ were simplify forced by carbon burial fluxes, observed changes in $[CO_3^{2-}]$ and calcite lysocline depth would be unacceptably large (Hoogakker et al., 2006). A possible resolution of this conundrum lies in concurrent changes in continental weathering and nutrient inputs, which would have opposing (i.e., mutually canceling) effects on deep-water $[CO_3^{2-}]$ but reinforcing effects on deep-ocean $\delta^{13}C$, which would decrease (increase) in response to enhanced (reduced) continental weathering and nutrient inputs. All of the hypotheses discussed above are permissive of concurrent changes in continental weathering and nutrient inputs (Ma et al., 2011).

4.4. Large-Amplitude Changes in Deep-Water $[CO_3^{2-}]$
4.4.1. $[CO_3^{2-}]$ Maximum at MIS 12/11 Boundary

The most notable feature of the MD06-3047B deep-water $[CO_3^{2-}]$ record may be the decrease of ~60 μmol kg^{-1} (from ~100 to 40 μmol kg^{-1}) between MIS 12/11 (~425 ka) and mid-MIS 11 (~400 ka), representing the largest change of this type during the past 700 kyr (Figure 5a). This peculiar interval also coincided with the largest change in the marine $\delta^{18}O$ record of the last 5 Myr (Lisiecki & Raymo, 2005) and has been described as a major step change in global climate conditions (Droxler et al., 2003).

Reconstructed deep-water $[CO_3^{2-}]$ from MD06-3047B reached its maximum of ~100 μmol kg^{-1} at the MIS12/11 termination (Figure 5a). Although the B/Ca-based $[CO_3^{2-}]$ profile from site ODP 806 (Kerr et al., 2017) does not show the same consistent increase at the MIS12/11 termination (Figure 5b), our result is consistent with "Pacific-style" CaCO$_3$ content records (Hodell et al., 2001), which also show their preservation maxima at the MIS 12/11 boundary (Figure 5c). A possible explanation for the missing $[CO_3^{2-}]$ maximum during the MIS 12/11 termination at site ODP 806 is that bioturbation has attenuated the deglacial signal in the Western Pacific Warm Pool, where sedimentation rates are typically low (Marchitto et al., 2005). Further high-resolution records in the deep Pacific Ocean are needed to confirm the MIS12/11 termination $[CO_3^{2-}]$ maximum as records of deep Pacific carbon chemistry are still relatively scarce. $[CO_3^{2-}]$/preservation maxima have been widely recognized during recent terminations in previous paleoceanographic studies (e.g., Berger, 1977; Mekik et al., 2012; Yu et al., 2010), and they have been interpreted to represent a breakdown of oceanic stratification (i.e., the "deglacial ventilation hypothesis"; Anderson et al., 2009; Martínez-Botí et al., 2015). In this hypothesis, increased overturning circulation leads to a transfer of carbon from the ocean to the atmosphere during deglaciations, thereby raising deep-water $[CO_3^{2-}]$ throughout the entire ocean (Boyle, 1988a,1988b). Our $[CO_3^{2-}]$ profile displays high values during deglaciations, consistent with the deglacial ventilation hypothesis. The extremely high $[CO_3^{2-}]$ values during the MIS 12/11 transition imply that the extent of oceanic carbon release during this interval was much larger than during other deglaciations since 700 ka.

The mid-Brunhes climatic shift (Jansen et al., 1986), which coincided with the MIS 12/11 transition, marked the onset of the late Quaternary regime of glacial cycles having warmer interglacials. The interglacials after MIS 11 were characterized by warmer climates (Jouzel et al., 2007; Lisiecki & Raymo, 2005) and higher atmospheric pCO$_2$ (Lüthi et al., 2008) than the preceding interglacials. This climate shift cannot be explained simply by orbital insolation forcing, because the insolation change during MIS 12/11 was relatively small (the "MIS 11 problem"; Imbrie & Imbrie, 1980). Because the mid-Brunhes climatic shift coincided with a significant deglacial carbon release from the Pacific Ocean, we infer that it may have been caused by a reorganization of the oceanic carbon system. During the last 800 kyr, atmospheric pCO$_2$ did not exceed 260 ppmv before MIS 11, but it reached ~280 ppmv for the first time after the deglacial carbon release of MIS 12/11 (Lüthi et al., 2008). Enhanced greenhouse gas forcing then made MIS 11 an unusually long and strong interglacial stage (Droxler et al., 2003). One problem with this explanation is that the extent of carbonate preservation during MIS 12/11 was not replicated during later deglaciations (Figure 5a). It is possible that the oceanic carbon release during MIS 12/11 crossed a climate threshold that changed internal Earth-system feedbacks.

4.4.2. [CO$_3^{2-}$] Minimum During the MBDI

The [CO$_3^{2-}$] minimum at ~400 ka, representing an intense global carbonate dissolution event, has been named the MBDI (see Barker et al., 2006 for summary). This dissolution event has been widely recorded in many proxies such as foraminiferal fragmentation (Flores et al., 2003; Le & Shackleton, 1992; Mix et al., 1995b), sediment CaCO$_3$ content (Farrell & Prell, 1989; Henrich et al., 2002; Hodell et al., 2001), relative abundance of benthic foraminifera (Mix et al., 1995b), coarse fraction percent (Bassinot et al., 1994; Chen & Farrell, 1991; Gröger et al., 2003; Prell, 1982), and B/Ca ratios of benthic foraminifera (Kerr et al., 2017; Sosdian et al., 2018). The MD06-3047B core provides a quantitative record of changes in deep-water [CO$_3^{2-}$] within the MBDI, documenting a decline to ~40 μmol kg^{-1} during MIS 11, which is ~10 μmol kg^{-1} lower than [CO$_3^{2-}$] minima during other interglacials of the last 700 kyr (Figure 7a). This is generally consistent with Kerr et al.'s (2017) result based on B/Ca ratios of the benthic foraminifer *C. wuellerstorfi* at nearby site ODP 806, where deep-water [CO$_3^{2-}$] shows a similar transient decline to ~30 μmol kg^{-1} at ~400 ka. A [CO$_3^{2-}$] of ~30–40 μmol kg^{-1} is roughly equal to that in the center of the modern North Pacific Deep Water, which has the lowest [CO$_3^{2-}$] in the global ocean.

The cause of the dissolution event during the MBDI has been widely discussed. Potential triggers of this event include unusually and persistently high sea-level elevations during MIS 11, global growth of modern barrier reefs, and global coccolithophore blooms during the mid-Brunhes interval. First, the unusually long sea-level highstand of MIS 11 (Droxler et al., 2003; Dutton et al., 2015; Olson & Hearty, 2009; Raynaud et al., 2003; Rohling et al., 2010; Figure 7b) would have transferred calcium carbonate from deep-ocean to shelf-carbonate reservoirs, causing a dissolution event in the deep ocean (Berger & Winterer, 1974). Second, many of the modern barrier reef systems, such as the Belize Barrier Reef (Figure 7c), were established during the mid-Brunhes interval (Droxler & Jorry, 2013; Montaggioni et al., 2011). A buildup of carbonate in barrier reefs in such large volumes also could have led to increased deep-ocean carbonate dissolution on a global scale (Berger, 1982). These two scenarios invoking increased shelf-carbonate production would have resulted in higher pCO$_2$ in the surface ocean, driving a net transfer of CO$_2$ from the ocean to the atmosphere. However, atmospheric pCO$_2$ was no higher during MIS 11 than in more recent interglacial stages (Lüthi et al., 2008; Figure 7e), as would be expected for a period of enhanced shelf-carbonate production (Berger, 1982). In order to explain the "CO$_2$ paradox" of MIS 11, Barker et al. (2006) proposed a third explanation, that is, that widespread dissolution during the MBDI was caused by a global increase in pelagic carbonate production associated with proliferation of the highly calcified coccolithophore *Gephyrocapsa*, triggering an increased organic carbon export flux owing to the ballast mineral effect (Figure 7d). In this way, fixation of organic carbon by the biological pump would have counteracted the rise in atmospheric pCO$_2$ expected from increased carbonate production during the MBDI. The MBDI was associated with a large change in the oceanic carbon system but little to no change in atmospheric pCO$_2$. The MD06-3047B core shows a [CO$_3^{2-}$] minimum during MIS 11 that was ~20 μmol kg^{-1} lower than the preindustrial Holocene value. If this change reflects a decline in mean deep-water [CO$_3^{2-}$] in the global ocean during the MBDI, the ~20-μmol kg^{-1} decrease in [CO$_3^{2-}$] would equate with an increase of pelagic carbonate production by 50%, according to the model of Barker et al. (2006). In summary, widespread carbonate dissolution during the MBDI is best explained by an increase in pelagic carbonate production due to coccolithophore blooms (Barker et al.,
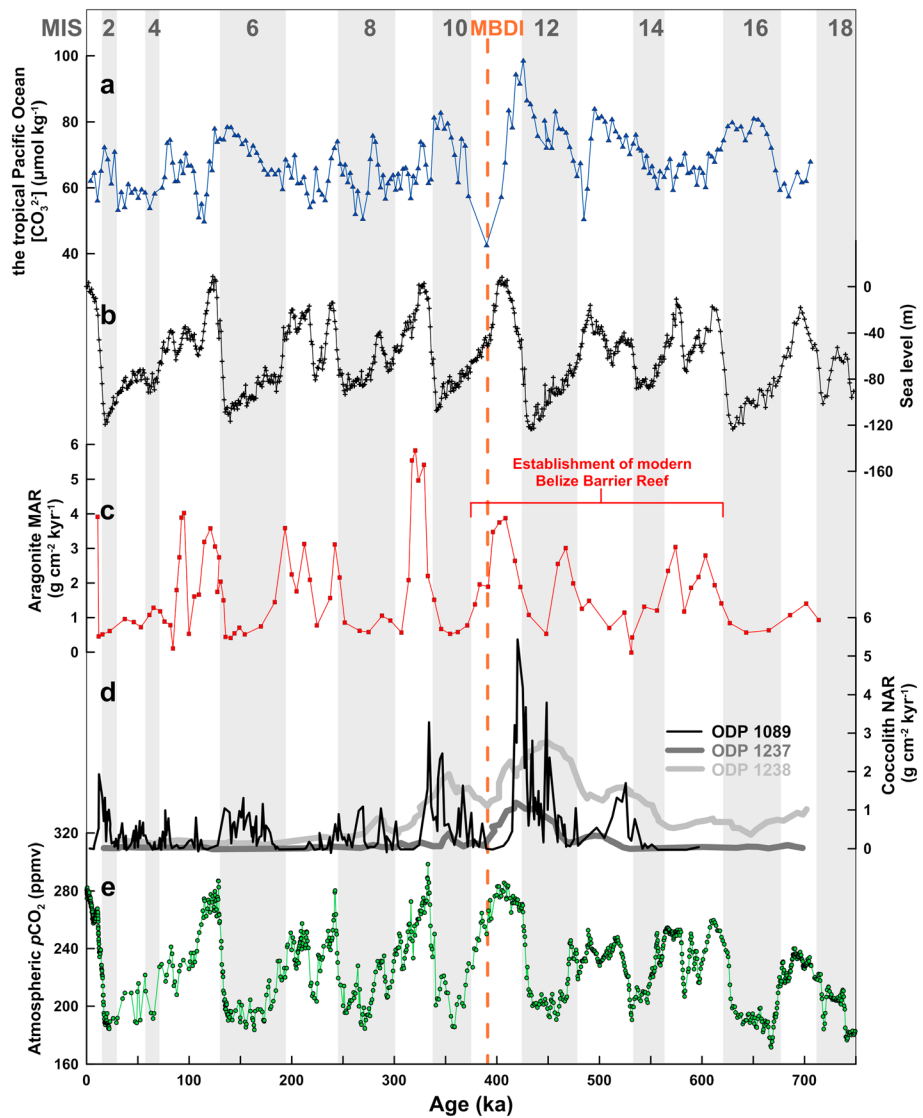
Figure 7. (a) Deep-water $[CO_3^{2-}]$ at site MD06-3047B in the western tropical Pacific (this study). (b) Global sea-level elevation (Miller et al., 2011). (c) Fine (<63 μm) aragonite mass accumulation rate at site MD02-2532 on the Belize margin (Droxler & Jorry, 2013). (d) Coccolith nannofossil accumulation rate for core ODP 1089 from the Atlantic Ocean (Flores et al., 2003) and for cores ODP 1237 and 1238 from the Pacific Ocean (Álvarez et al., 2010). (e) Atmospheric pCO_2 (Lüthi et al., 2008). The dashed line indicates the mid-Brunhes dissolution interval.

2006). A ~50% increase in pelagic carbonate production (compared to preindustrial levels) could theoretically account for the entire $[CO_3^{2-}]$ decrease during the MBDI.

4.5. $[CO_3^{2-}]$ Increases During MIS 3–2 and MIS 13

The MD06-3047B $[CO_3^{2-}]$ profile exhibits two striking anomalies from MIS 3 to MIS 2 and from early to middle MIS 13, when compared to "Pacific-style" deep-sea sedimentary carbonate cycles (Hodell et al., 2001). In this study, the 2.5-km-deep study site displays a clear increase in $[CO_3^{2-}]$ from MIS 3 to MIS 2, which is in contrast to the carbonate content record of Site ODP 1089 (48°S; 10°E; 4.6-km water depth; Figures 5a and 5c). A recent B/Ca-based $[CO_3^{2-}]$ reconstruction at a comparable water depth (ODP 806, 2.5-km deep) in the western tropical Pacific Ocean also displays a rising trend from MIS 3 to MIS 2 (Kerr et al., 2017; Figure 5b), in agreement with the $[CO_3^{2-}]$ record at site MD06-3047B. Considering site ODP 1089 is bathed by lower CDW and its carbonate content reflects qualitative, high-resolution changes in deep Pacific $[CO_3^{2-}]$ (Hodell

et al., 2001), the opposite patterns of variation in $[CO_3^{2-}]$ at intermediate (MD06-3047B and ODP 806) and deep (ODP 1089) sites imply a change in the structure of watermasses in the western tropical Pacific. This inference is consistent with the argument of Yu et al. (2013) that enhanced vertical oceanic stratification was responsible for the increased gradient in $[CO_3^{2-}]$ between intermediate (2.3 km) and deep (>3.4 km) waters in the tropical Pacific Ocean from MIS 3 to MIS 2. This result from the tropical Pacific is also consistent with $[CO_3^{2-}]$ records from the South Atlantic and Southwest Pacific Oceans, which are interpreted to reflect greater stratification during MIS 2 (Allen et al., 2015; Yu et al., 2014). Enhanced water-column stratification would have contributed to sequestration of a larger proportion of respired carbon in the deep ocean, thereby contributing to the final step of atmospheric CO_2 drawdown during the last glaciation (Yu et al., 2013).

A rising trend in $[CO_3^{2-}]$ is also observed from the early to the middle part of MIS 13 at site MD06-3047B, which is in contrast to the decreasing carbonate content at Site 1089 (Hodell et al., 2001; Figures 5a and 5c). An increased vertical $[CO_3^{2-}]$ gradient during MIS 13 suggests that the deep Pacific stratification scenario also applies to this time interval. This suggestion, however, requires further confirmation by high resolution $[CO_3^{2-}]$ records from the deep Pacific Ocean, as our record is currently the only existing $[CO_3^{2-}]$ deep-Pacific reconstruction for MIS 13. Ice-core records suggest that MIS 13 was an interglacial period with cooler Antarctic temperatures (Jouzel et al., 2007) and lower CO_2 and CH_4 concentrations than those recorded in the preceding and subsequent interglacials (Loulergue et al., 2008; Luthi et al., 2008). Based on the compiled ice, marine, and terrestrial palaeoclimate records from around the globe, MIS 13 was clearly the weakest interglacial of the last 800 kyr (Lang & Wolff, 2011; PAGES, 2016). Therefore, we infer that increased stratification in the deep Pacific Ocean may partially explain lower atmospheric CO_2 concentrations during MIS 13, resulting in weak interglacial intensity. In summary, $[CO_3^{2-}]$ at site MD06-3047B shows increases from MIS 3 to MIS 2 and from early to mid-MIS 13, in contrast with the previous $[CO_3^{2-}]$ reconstructions at relatively deeper sites in the Pacific Ocean (Hodell et al., 2001; Yu et al., 2013). The enhanced vertical chemical gradient suggested by these data implies greater Pacific Ocean stratification during these two intervals.

5. Conclusions

An SNW-based reconstruction of deep-water $[CO_3^{2-}]$ for the western tropical Pacific since 700 ka yields the following conclusions:

(1) Our $[CO_3^{2-}]$ data reveal a negative correlation with sea-level elevations on glacial-interglacial time scales, supporting the "coral reef hypothesis" that the deep Pacific carbonate system responded to variations in shelf-carbonate production through the past 700 kyr.

(2) Deep-water $[CO_3^{2-}]$ shows no 400- to 500-kyr cycles in benthic foraminiferal $\delta^{13}C$ records globally, at least over the last 700 kyr. A possible resolution of this conundrum lies in concurrent changes in continental weathering and nutrient inputs, which would have had opposing effects on deep-water $[CO_3^{2-}]$ but reinforcing effects on deep-ocean $\delta^{13}C$.

(3) Large-amplitude changes in deep Pacific $[CO_3^{2-}]$ during the mid-Brunhes interval are revealed by our quantitative $[CO_3^{2-}]$ record. A $[CO_3^{2-}]$ maximum of ~100 μmol kg^{-1} at the MIS12/11 termination records the largest deglacial oceanic carbon release since 700 ka. $[CO_3^{2-}]$ declined to ~40 μmol kg^{-1} during the MBDI centered on MIS 11, in response to global increases in pelagic-carbonate production.

(4) The increases in $[CO_3^{2-}]$ gradient between intermediate (2.5 km, this study) and deep (>3.4 km, Hodell et al., 2001; Yu et al., 2013) Pacific waters from MIS 3 to 2 and from early to mid-MIS 13 imply greater Pacific stratification during these two intervals.

References

Adkins, J. F. (2013). The role of deep ocean circulation in setting glacial climates. *Paleoceanography*, *28*, 539–561. https://doi.org/10.1002/palo.20046

Allen, K. A., Sikes, E. L., Hönisch, B., Elmore, A. C., Guilderson, T. P., Rosenthal, Y., & Anderson, R. F. (2015). Southwest Pacific deep water carbonate chemistry linked to high southern latitude climate and atmospheric CO_2 during the last glacial termination. *Quaternary Science Reviews*, *122*, 180–191. https://doi.org/10.1016/j.quascirev.2015.05.007

Álvarez, M. C., Flores, J. A., Sierro, F. J., & Molina-Cruz, A. (2010). Long-term upwelling evolution in tropical and equatorial Pacific during the last 800 kyr as revealed by coccolithophore assemblages. *Géobios*, *43*(1), 123–130. https://doi.org/10.1016/j.geobios.2009.07.001

Anderson, R. F., Ali, S., Bradtmiller, L. I., Nielsen, S. H. H., Fleisher, M. Q., Anderson, B. E., & Burckle, L. H. (2009). Wind-driven upwelling in the Southern Ocean and the deglacial rise in atmospheric CO_2. *Science*, *323*(5920), 1443–1448. https://doi.org/10.1126/science.1167441

Anderson, R. F., Fleisher, M., Lao, Y., & Winckler, G. (2008). Modern $CaCO_3$ preservation in equatorial Pacific sediments in the context of late-Pleistocene glacial cycles. *Marine Chemistry*, *111*(1), 30–46. https://doi.org/10.1016/j.marchem.2007.11.011

Archer, D., Emerson, S., & Reimers, C. (1989). Dissolution of calcite in deep-sea sediments: pH and O_2 microelectrode results. *Geochimica et Cosmochimica Acta*, *53*(11), 2831–2845. https://doi.org/10.1016/0016-7037(89)90161-0

Archer, D., & Maier-Reimer, E. (1994). Effect of deep-sea sedimentary calcite preservation on atmospheric CO_2 concentration. *Nature*, *367*(6460), 260–263. https://doi.org/10.1038/367260a0

Armstrong, R. A., Lee, C., Hedges, J. I., Honjo, S., & Wakeham, S. G. (2001). A new, mechanistic model for organic carbon fluxes in the ocean based on the quantitative association of POC with ballast minerals. *Deep Sea Research Part II: Topical Studies in Oceanography*, *49*(1-3), 219–236. https://doi.org/10.1016/S0967-0645(01)00101-1

Barker, S., Archer, D., Booth, L., Elderfield, H., Henderiks, J., & Rickaby, R. E. M. (2006). Globally increased pelagic carbonate production during the mid-Brunhes dissolution interval and the CO_2 paradox of MIS 11. *Quaternary Science Reviews*, *25*(23–24), 3278–3293. https://doi.org/10.1016/j.quascirev.2006.07.018

Barker, S., & Elderfield, H. (2002). Foraminiferal calcification response to glacial-interglacial changes in atmospheric CO_2. *Science*, *297*(5582), 833–836. https://doi.org/10.1126/science.1072815

Bassinot, F. C., Beaufort, L., Vincent, E., Labeyrie, L. D., Rostek, F., Miiller, P. J., et al. (1994). Coarse fraction fluctuations in pelagic carbonate sediments from the tropical Indian Ocean: A 1,500 kyr record of carbonate dissolution. *Paleoceanography*, *9*(4), 579–600. https://doi.org/10.1029/94PA00860

Berger, W. H. (1973). Deep-sea carbonates; Pleistocene dissolution cycles. *Journal of Foraminiferal Research*, *3*(4), 187–195. https://doi.org/10.2113/gsjfr.3.4.187

Berger, W. H. (1977). Deep-sea carbonate and the deglaciation preservation spike in pteropods and foraminifera. *Nature*, *269*(5626), 301–304. https://doi.org/10.1038/269301a0

Berger, W. H. (1982). Increase of carbon dioxide in the atmosphere during deglaciation: The coral reef hypothesis. *Naturwissenschaften*, *69*(2), 87–88. https://doi.org/10.1007/BF00441228

Berger, W. H., & Winterer, E. (1974). Plate stratigraphy and the fluctuating carbonate line. *Pelagic sediments: on land and under the sea*, 11–48. https://doi.org/10.1002/9781444304855.ch2

Bickert, T., Berger, W. H., Burke, S., Schmidt, H., & Wefer, G. (1993). Late Quaternary stable isotope record of benthic foraminifers: Sites 805 and 806, Ontong Java Plateau. In W. H. Berger, et al. (Eds.), *Proceedings of the Ocean Drilling Program, Scientific Results* (Vol. 130, pp. 411–420). College Station, TX (Ocean Drilling Program). https://doi.org/10.2973/odp.proc.sr.130.025.1993

Bordiga, M., Beaufort, L., Cobianchi, M., Lupi, C., Mancin, N., Luciani, V., et al. (2013). Calcareous plankton and geochemistry from the ODP site 1209B in the NW Pacific Ocean (Shatsky Rise): New data to interpret calcite dissolution and paleoproductivity changes of the last 450 ka. *Palaeogeography Palaeoclimatology Palaeoecology*, *371*(2), 93–108. https://doi.org/10.1016/j.palaeo.2012.12.021

Boyle, E. A. (1988a). The role of vertical chemical fractionation in controlling late Quaternary atmospheric carbon dioxide. *Journal of Geophysical Research*, *93*(C12), 15,701–15,714. https://doi.org/10.1029/JC093iC12p15701

Boyle, E. A. (1988b). Vertical oceanic nutrient fractionation and glacial/interglacial CO_2 cycles. *Nature*, *331*(6151), 55–56. https://doi.org/10.1038/331055a0

Broecker, W. S., & Clark, E. (2001). An evaluation of Lohmann's foraminifera weight dissolution index. *Paleoceanography*, *16*(5), 531–534. https://doi.org/10.1029/2000PA000600

Broecker, W. S., & Peng, T. H. (1987). The role of $CaCO_3$ compensation in the glacial to interglacial atmospheric CO_2 change. *Global Biogeochemical Cycles*, *1*(1), 15–29. https://doi.org/10.1029/GB001i001p00015

Brunelle, B. G., Sigman, D. M., Cook, M. S., Keigwin, L. D., Haug, G. H., Plessen, B., et al. (2007). Evidence from diatom-bound nitrogen isotopes for subarctic Pacific stratification during the last ice age and a link to North Pacific denitrification changes. *Paleoceanography*, *22*, PA1215. https://doi.org/10.1029/2005PA001205

Chen, J., Farrell, J. W., Murray, D. W., & Prell, W. L. (1995). Timescale and paleoceanographic implications of a 3.6 m.y. oxygen isotope record from the Northeast Indian Ocean (ocean drilling program site 758). *Paleoceanography*, *10*(1), 21–47. https://doi.org/10.1029/94PA02290

Chen, M. T., & Farrell, J. W. (1991). Planktonic foraminifer faunal variations in the northeastern Indian Ocean: A high-resolution record of the past 800,000 years from site 758. *Proceeding of the Ocean Drilling Program, Scientific Results*, *121*, 125–140.

Chiu, T. C., & Broecker, W. S. (2008). Toward better paleocarbonate ion reconstructions: New insights regarding the $CaCO_3$ size index. *Paleoceanography*, *23*, PA2216. https://doi.org/10.1029/2008PA001599

De Villiers, S. (2004). Optimum growth conditions as opposed to calcite saturation as a control on the calcification rate and shell-weight of marine foraminifera. *Marine Biology*, *144*(1), 45–49. https://doi.org/10.1007/s00227-003-1183-8

Dickson, A. G. (1990). Thermodynamics of the dissociation of boric acid in synthetic seawater from 273.15 to 318.15 K. *Deep Sea Research Part A. Oceanographic Research Papers*, *37*(5), 755–766. https://doi.org/10.1016/0198-0149(90)90004-F

Droxler, A. W., Alley, R. B., Howard, W. R., Poore, R. Z., & Burckle, L. H. (2003). Unique and exceptionally long interglacial marine isotope stage 11: Window into Earth warm future climate. *Earth's Climate and Orbital Eccentricity: The Marine Isotope Stage 11 Question*, 1–14. https://doi.org/10.1029/137GM01

Droxler, A. W., & Jorry, S. J. (2013). Deglacial origin of barrier reefs along low-latitude mixed siliciclastic and carbonate continental shelf edges. *Annual Review of Marine Science*, *5*(1), 165–190. https://doi.org/10.1146/annurev-marine-121211-172234

Dutton, A., Carlson, A. E., Long, A. J., Milne, G. A., Clark, P. U., Deconto, R., et al. (2015). Sea-level rise due to polar ice-sheet mass loss during past warm periods. *Science*, *349*(6244), aaa4019. https://doi.org/10.1126/science.aaa4019

Farrell, J. W., & Prell, W. L. (1989). Climatic change and $CaCO_3$ preservation: An 800,000 year bathymetric reconstruction from the central equatorial Pacific Ocean. *Paleoceanography*, *4*(4), 447–466. https://doi.org/10.1029/PA004i004p00447

Ferrari, R., Jansen, M. F., Adkins, J. F., Burke, A., Stewart, A. L., & Thompson, A. F. (2014). Antarctic Sea ice control on ocean circulation in present and glacial climates. *Proceedings of the National Academy of Sciences*, *111*(24), 8753–8758. https://doi.org/10.1073/pnas.1323922111

Flores, J. A., Marino, M., Sierro, F. J., Hodell, D. A., & Charles, C. D. (2003). Calcareous plankton dissolution pattern and coccolithophore assemblages during the last 600 kyr at ODP site 1089 (Cape Basin, South Atlantic): Paleoceanographic implications. *Palaeogeography Palaeoclimatology Palaeoecology*, *196*(3-4), 409–426. https://doi.org/10.1016/S0031-0182(03)00467-X

Gebhardt, H., Sarnthein, M., Grootes, P. M., Kiefer, T., Kuehn, H., Schmieder, F., & Röhl, U. (2008). Paleonutrient and productivity records from the subarctic North Pacific for Pleistocene glacial terminations I to V. *Paleoceanography*, *23*, PA4212. https://doi.org/10.1029/2007PA001513

Grant, K. M., Rohling, E. J., Ramsey, C. B., Cheng, H., Edwards, R. L., Florindo, F., et al. (2014). Sea-level variability over five glacial cycles. *Nature Communications*, *5*(1), 5076. https://doi.org/10.1038/ncomms6076

Gröger, M., Henrich, R., & Bickert, T. (2003). Glacial-interglacial variability in lower North Atlantic Deep Water: Inference from silt grain-size analysis and carbonate preservation in the western equatorial Atlantic. *Marine Geology*, *201*(4), 321–332. https://doi.org/10.1016/S0025-3227(03)00263-9

Hall, I. R., McCave, I. N., Shackleton, N. J., Weedon, G. P., & Harris, S. E. (2001). Intensified deep Pacific inflow and ventilation in Pleistocene glacial times. *Nature*, *412*(6849), 809–812. https://doi.org/10.1038/35090552

Haug, G. H., Sigman, D. M., Tiedemann, R., Pedersen, T. F., & Sarnthein, M. (1999). Onset of permanent stratification in the subarctic Pacific Ocean. *Nature*, *401*(6755), 779–782. https://doi.org/10.1038/44550

Henrich, R., Baumann, K. H., Huber, R., & Meggers, H. (2002). Carbonate preservation records of the past 3 Myr in the Norwegian-Greenland Sea and the northern North Atlantic: Implications for the history of NADW production. *Marine Geology*, *184*(1-2), 17–39. https://doi.org/10.1016/S0025-3227(01)00279-1

Hodell, D., Charles, C., & Sierro, F. (2001). Late Pleistocene evolution of the ocean's carbonate system. *Earth and Planetary Science Letters*, *192*(2), 109–124. https://doi.org/10.1016/S0012-821X(01)00430-7

Hoogakker, B. A. A., Rohling, E. J., Palmer, M. R., Tyrrell, T., & Rothwell, R. G. (2006). Underlying causes for long-term global ocean δ^{13}C fluctuations over the last 1.20 Myr. *Earth and Planetary Science Letters*, *248*(1–2), 15–29. https://doi.org/10.1016/j.epsl.2006.05.007

Imbrie, J., & Imbrie, J. Z. (1980). Modeling the climatic response to orbital variations. *Science*, *207*(4434), 943–953. https://doi.org/10.1126/science.207.4434.943

Jaccard, S., Haug, G., Sigman, D., Pedersen, T., Thierstein, H., & Röhl, U. (2005). Glacial/interglacial changes in subarctic North Pacific stratification. *Science*, *308*(5724), 1003–1006. https://doi.org/10.1126/science.1108696

Jansen, J. H. F., Kuijpers, A., & Troelstra, S. R. (1986). A mid-Brunhes climatic event: Long-term changes in global atmosphere and ocean circulation. *Science*, *232*(4750), 619–622. https://doi.org/10.1126/science.232.4750.619

Jia, Q., Li, T., Xiong, Z., & Chang, F. (2015). Foraminiferal carbon and oxygen isotope composition characteristics and their paleoceanographic implications in the north margin of the western Pacific warm pool over the past about 700,000 years (in Chinese with English abstract). *Quaternary Sciences*, *35*, 401–410. https://doi.org/10.11928/j.issn.1001-7410.2015.02.15

Jia, Q., Li, T., Xiong, Z., Steinke, S., Jiang, F., Chang, F., & Qin, B. (2018). Hydrological variability in the western tropical Pacific over the past 700 kyr and its linkage to Northern Hemisphere climatic change. *Palaeogeography Palaeoclimatology Palaeoecology*, *493*, 44–54. https://doi.org/10.1016/j.palaeo.2017.12.039

Jouzel, J., Massondelmotte, V., Cattani, O., Dreyfus, G., Falourd, S., Hoffmann, G., et al. (2007). Orbital and millennial Antarctic climate variability over the past 800,000 years. *Science*, *317*(5839), 793–796. https://doi.org/10.1126/science.1141038

Keigwin, L. D., & Boyle, E. A. (1985). Carbon isotopes in deep-sea benthic foraminifera: Precession and changes in low-latitude biomass. *Washington Dc American Geophysical Union Geophysical Monograph*, 319–328. https://doi.org/10.1029/GM032p0319

Kerr, J., Rickaby, R., Yu, J., Elderfield, H., & Sadekov, A. Y. (2017). The effect of ocean alkalinity and carbon transfer on deep-sea carbonate ion concentration during the past five glacial cycles. *Earth and Planetary Science Letters*, *471*, 42–53. https://doi.org/10.1016/j.epsl.2017.04.042

Key, R. M., Kozyr, A., Sabine, C. L., Lee, K., Wanninkhof, R., Bullister, J. L., et al. (2004). A global ocean carbon climatology: Results from Global Data Analysis Project (GLODAP). *Global Biogeochemical Cycles*, *18*, GB4031. https://doi.org/10.1029/2004GB002247

Klaas, C., & Archer, D. E. (2002). Association of sinking organic matter with various types of mineral ballast in the deep sea: Implications for the rain ratio. *Global Biogeochemical Cycles*, *16*(4), 1116. https://doi.org/10.1029/2001GB001765

Lalicata, J. J., & Lea, D. W. (2011). Pleistocene carbonate dissolution fluctuations in the eastern equatorial Pacific on glacial timescales: Evidence from ODP hole 1241. *Fuel and Energy Abstracts*, *79*(1–2), 41–51. https://doi.org/10.1016/j.marmicro.2011.01.002

Lang, N., & Wolff, E. W. (2011). Interglacial and glacial variability from the last 800 ka in marine, ice and terrestrial archives. *Climate of the Past*, *7*(2), 361–380. https://doi.org/10.5194/cp-7-361-2011

Le, J., & Shackleton, N. J. (1992). Carbonate dissolution fluctuations in the western equatorial Pacific during the late Quaternary. *Paleoceanography*, *7*(1), 21–42. https://doi.org/10.1029/91PA02854

Lear, C. H., Billups, K., Rickaby, R. E. M., Diesterhaass, L., Mawbey, E. M., & Sosdian, S. M. (2016). Breathing more deeply: Deep ocean carbon storage during the mid-Pleistocene climate transition. *Geology*, *44*(12), 1035–1038. https://doi.org/10.1130/G38636.1

Levitus, S., Antonov, J., Baranova, O. K., Boyer, T., Coleman, C., Garcia, H., et al. (2013). The world ocean database. *Data Science Journal*, *12*(0), WDS229–WDS234.

Li, T., Zhao, J., Nan, Q., Sun, R., & Yu, X. (2011). Palaeoproductivity evolution in the centre of the western Pacific warm pool during the last 250 ka. *Journal of Quaternary Science*, *26*(5), 478–484. https://doi.org/10.1002/jqs.1471

Lisiecki, L. E., & Raymo, M. E. (2005). A Pliocene-Pleistocene stack of 57 globally distributed benthic δ^{18}O records. *Paleoceanography*, *20*, PA1003. https://doi.org/10.1029/2004PA001071

Lohmann, G. (1995). A model for variation in the chemistry of planktonic foraminifera due to secondary calcification and selective dissolution. *Paleoceanography*, *10*(3), 445–457. https://doi.org/10.1029/95PA00059

Loulergue, L., Schilt, A., Spahni, R., Masson-Delmotte, V., Blunier, T., Lemieux, B., et al. (2008). Orbital and millennial-scale features of atmospheric CH_4 over the past 800,000 years. *Nature*, *453*(7193), 383–386. https://doi.org/10.1038/nature06950

Lüthi, D., Le Floch, M., Bereiter, B., Blunier, T., Barnola, J. M., Siegenthaler, U., et al. (2008). High-resolution carbon dioxide concentration record 650,000-800,000 years before present. *Nature*, *453*(7193), 379–382. https://doi.org/10.1038/nature06949

Ma, W., Tian, J., Li, Q., & Wang, P. (2011). Simulation of long eccentricity (400-kyr) cycle in ocean carbon reservoir during Miocene Climate Optimum: Weathering and nutrient response to orbital change. *Geophysical Research Letters*, *38*, L10701. https://doi.org/10.1029/2011GL047680

Ma, W., Wang, P., & Tian, J. (2017). Modeling 400-500-kyr Pleistocene carbon isotope cyclicity through variations in the dissolved organic carbon pool. *Global and Planetary Change*, *152*, 187–198. https://doi.org/10.1016/j.gloplacha.2017.04.001

Marchitto, T. M., Lynch-Stieglitz, J., & Hemming, S. R. (2005). Deep Pacific $CaCO_3$ compensation and glacial–interglacial atmospheric CO_2. *Earth and Planetary Science Letters*, *231*(3-4), 317–336. https://doi.org/10.1016/j.epsl.2004.12.024

Martínez-Botí, M. A., Marino, G., Foster, G. L., Ziveri, P., Henehan, M. J., Rae, J. W., et al. (2015). Boron isotope evidence for oceanic carbon dioxide leakage during the last deglaciation. *Nature*, *518*(7538), 219–222. https://doi.org/10.1038/nature14155

McCave, I. N., Carter, L., & Hall, I. R. (2008). Glacial-interglacial changes in water mass structure and flow in the SW Pacific Ocean. *Quaternary Science Reviews*, *27*(19-20), 1886–1908. https://doi.org/10.1016/j.quascirev.2008.07.010

McCave, I. N., Manighetti, B., & Robinson, S. G. (1995). Sortable silt and fine sediment size/composition slicing: Parameters for palaeocurrent speed and palaeoceanography. *Paleoceanography*, *10*(3), 593–610. https://doi.org/10.1029/94PA03039

Mehrbach, C. (1973). Measurement of the apparent dissociation constants of carbonic acid in seawater at atmospheric pressure. *Limnology and Oceanography*, *18*(6), 897–907. https://doi.org/10.4319/lo.1973.18.6.0897

Mekik, F. A., Anderson, R. F., Loubere, P., François, R., & Richaud, M. (2012). The mystery of the missing deglacial carbonate preservation maximum. *Quaternary Science Reviews*, *39*, 60–72. https://doi.org/10.1016/j.quascirev.2012.01.024

Miller, K. G., Mountain, G. S., Wright, J. D., & Browning, J. V. (2011). A 180-million-year record of sea level and ice volume variations from continental margin and deep-sea isotopic records. *Oceanography*, *24*(2), 40–53. https://doi.org/10.5670/oceanog.2011.26

Mix, A. C., Le, J., & Shackleton, N. J. (1995a). Benthic foraminiferal stable isotope stratigraphy of site 846: 0-1.8 Ma. *Proceeding of the Ocean Drilling Program, Scientific Results*, *138*, 839–854.

Mix, A. C., Le, J., & Shackleton, N. J. (1995b). Late Quaternary paleoceanography in the eastern equatorial Pacific Ocean from planktonic foraminifers: A high-resolution record from site 846. *Journal of Cardiovascular Electrophysiology*, *15*(10), 1111–1117.

Mix, A. C., Pisias, N. G., Rugh, W., Wilson, J., Morey, A., & Hagelberg, T. K. (1995). Benthic foraminifer stable isotope record from site 849 (0-5 Ma): Local and global climate changes. *Proceeding of the Ocean Drilling Program, Scientific Results*, *138*, 371–412.

Montaggioni, L. F., Cabioch, G., Thouveny, N., Frank, N., Sato, T., & Sémah, A. M. (2011). Revisiting the quaternary development history of the western New Caledonian shelf system: From ramp to barrier reef. *Marine Geology*, *280*(1-4), 57–75. https://doi.org/10.1016/j.margeo.2010.12.001

Moy, A. D., Howard, W. R., Bray, S. G., & Trull, T. W. (2009). Reduced calcification in modern Southern Ocean planktonic foraminifera. *Nature Geoscience*, *2*(4), 276–280. https://doi.org/10.1038/ngeo460

Naik, S. S., Naidu, P. D., Govil, P., & Godad, S. (2010). Relationship between weights of planktonic foraminifer shell and surface water $CO_3^=$ concentration during the Holocene and Last Glacial Period. *Marine Geology*, *275*(1–4), 278–282. https://doi.org/10.1016/j.margeo.2010.05.004

Nath, B. N., Sijinkumar, A. V., Borole, D. V., Gupta, S. M., Mergulhao, L. P., Mascarenhas-Pereira, M. B. L., et al. (2013). Record of carbonate preservation and the mid-Brunhes climatic shift from a seamount top with low sedimentation rates in the central Indian Basin. *Boreas*, *42*(3), 762–778. https://doi.org/10.1111/j.1502-3885.2012.00304.x

Ninnemann, U. S., & Charles, C. D. (2002). Changes in the mode of Southern Ocean circulation over the last glacial cycle revealed by foraminiferal stable isotopic variability. *Earth and Planetary Science Letters*, *201*(2), 383–396. https://doi.org/10.1016/S0012-821X(02)00708-2

Olson, S. L., & Hearty, P. J. (2009). A sustained +21 m sea-level highstand during MIS 11 (400 ka): Direct fossil and sedimentary evidence from Bermuda. *Quaternary Science Reviews*, *28*(3–4), 271–285. https://doi.org/10.1016/j.quascirev.2008.11.001

Oppo, D. W., Raymo, M. E., Lohmann, G. P., Mix, A. C., Wright, J. D., & Prell, W. L. (1995). A δ^{13}C record of upper North Atlantic Deep Water during the past 2.6 million years. *Paleoceanography*, *10*(3), 373–394. https://doi.org/10.1029/95PA00332

PAGES (Past Interglacials Working Group of PAGES) (2016). Interglacials of the last 800,000 years. *Reviews of Geophysics*, *54*, 162–219. https://doi.org/10.1002/2015RG000482

Pelletier, G., Lewis, E., & Wallace, D. (2007). *CO2Sys. xls: A calculator for the CO2 system in seawater for microsoft excel/VBA*. Olympia, WA/Upton, NY, USA: Washington State Department of Ecology/Brookhaven National Laboratory.

Prell, W. L. (1982). Oxygen and carbon isotope stratigraphy for the Quaternary of hole 502B: Evidence for two modes of isotopic variability. *Initial Reports DSDP*, *68*, 455–464.

Qin, B., Li, T., Xiong, Z., Algeo, T. J., & Chang, F. (2016). An improved protocol for cleaning of planktonic foraminifera for shell weight measurement. *Journal of Sedimentary Research*, *86*(5), 431–437. https://doi.org/10.2110/jsr.2016.31

Qin, B., Li, T., Xiong, Z., Algeo, T. J., & Chang, F. (2017). Deepwater carbonate ion concentrations in the western tropical Pacific since 250 ka: Evidence for oceanic carbon storage and global climate influence. *Paleoceanography*, *32*, 351–370. https://doi.org/10.1002/2016PA003039

Raynaud, D., Loutre, M. F., Ritz, C., Barnola, J. M., Berger, A., Chappellaz, J., et al. (2003). Marine isotope stage (MIS) 11 in the Vostok ice core: CO_2 forcing and stability of East Antarctica. *Earth's Climate and Orbital Eccentricity: The Marine Isotope Stage 11 Question*, 27–40. https://doi.org/10.1029/137GM03

Rickaby, R. E. M., Bard, E., Sonzogni, C., Rostek, F., Beaufort, L., Barker, S., et al. (2007). Coccolith chemistry reveals secular variations in the global ocean carbon cycle? *Earth and Planetary Science Letters*, *253*(1–2), 83–95. https://doi.org/10.1016/j.epsl.2006.10.016

Rickaby, R. E. M., Elderfield, H., Roberts, N., Hillenbrand, C. D., & Mackensen, A. (2010). Evidence for elevated alkalinity in the glacial Southern Ocean. *Paleoceanography*, *25*, PA1209. https://doi.org/10.1029/2009PA001762

Rippert, N., Nürnberg, D., Raddatz, J., Maier, E., Hathorne, E., Bijma, J., & Tiedemann, R. (2016). Constraining foraminiferal calcification depths in the western Pacific warm pool. *Marine Micropaleontology*, *128*, 14–27. https://doi.org/10.1016/j.marmicro.2016.08.004

Rohling, E. J., Braun, K., Grant, K., Kucera, M., Roberts, A. P., Siddall, M., & Trommer, G. (2010). Comparison between Holocene and marine isotope Stage-11 sea-level histories. *Earth and Planetary Science Letters*, *291*(1–4), 97–105. https://doi.org/10.1016/j.epsl.2009.12.054

Russon, T., Paillard, D., & Elliot, M. (2010). Potential origins of 400-500 kyr periodicities in the ocean carbon cycle: A box model approach. *Global Biogeochemical Cycles*, *24*, GB2013. https://doi.org/10.1029/2009GB003586

Sexton, P. F., & Barker, S. (2012). Onset of 'Pacific-style' deep-sea sedimentary carbonate cycles at the mid-Pleistocene transition. *Earth and Planetary Science Letters*, *321-322*, 81–94. https://doi.org/10.1016/j.epsl.2011.12.043

Sigman, D. M., Hain, M. P., & Haug, G. H. (2010). The polar ocean and glacial cycles in atmospheric CO_2 concentration. *Nature*, *466*(7302), 47–55. https://doi.org/10.1038/nature09149

Sosdian, S. M., Rosenthal, Y., & Toggweiler, J. R. (2018). Deep Atlantic carbonate ion and $CaCO_3$ compensation during the ice ages. *Paleoceanography and Paleoclimatology*, *33*(6), 546–562. https://doi.org/10.1029/2017PA003312

Tian, J., Xie, X., Ma, W., Jin, H., & Wang, P. (2011). X-ray fluorescence core scanning records of chemical weathering and monsoon evolution over the past 5 Myr in the southern South China Sea. *Paleoceanography*, *26*, PA4202. https://doi.org/10.1029/2010PA002045

Wang, P., Li, Q., Tian, J., Jian, Z., Liu, C., Li, L., & Ma, W. (2014). Long-term cycles in the carbon reservoir of the Quaternary Ocean: A perspective from the South China Sea. *National Science Review*, *1*(1), 119–143. https://doi.org/10.1093/nsr/nwt028

Wang, P., Tian, J., Cheng, X., Liu, C., & Xu, J. (2003). Carbon reservoir changes preceded major ice-sheet expansion at the mid-Brunhes event. *Geology*, *31*(3), 239–242. https://doi.org/10.1130/0091-7613(2003)031<0239:CRCPMI>2.0.CO;2

Wang, P., Tian, J., Cheng, X., Liu, C., & Xu, J. (2004). Major Pleistocene stages in a carbon perspective: The South China Sea record and its global comparison. *Paleoceanography*, *19*, PA4005. https://doi.org/10.1029/2003PA000991

Wu, G., Herguera, J. C., & Berger, W. H. (1990). Differential dissolution: Modification of Late Pleistocene oxygen isotope records in the western equatorial Pacific. *Paleoceanography*, *5*(4), 581–594. https://doi.org/10.1029/PA005i004p00581

Yasuda, M., Berger, W. H., Wu, G., Burke, S., & Schmidt, H. (1993). Foraminifer preservation record for the last million years: Site 805. *Proceeding of the Ocean Drilling Program, Scientific Results*, *130*, 491–508.

Yu, J., Anderson, R. F., Jin, Z., Rae, J. W., Opdyke, B. N., & Eggins, S. M. (2013). Responses of the deep ocean carbonate system to carbon reorganization during the Last Glacial-interglacial cycle. *Quaternary Science Reviews*, *76*, 39–52. https://doi.org/10.1016/j.quascirev.2013.06.020

Yu, J., Anderson, R. F., & Rohling, E. J. (2014). Deep ocean carbonate chemistry and glacial-interglacial atmospheric CO_2 changes. *Oceanography*, *27*(1), 16–25. https://doi.org/10.5670/oceanog.2014.04

Yu, J., Broecker, W. S., Elderfield, H., Jin, Z., McManus, J., & Zhang, F. (2010). Loss of carbon from the deep sea since the Last Glacial Maximum. *Science*, *330*(6007), 1084–1087. https://doi.org/10.1126/science.1193221

Yu, J., & Elderfield, H. (2007). Benthic foraminiferal B/Ca ratios reflect deep water carbonate saturation state. *Earth and Planetary Science Letters*, *258*(1-2), 73–86. https://doi.org/10.1016/j.epsl.2007.03.025

Zhang, J., Wang, P., Li, Q., Cheng, X., Jin, H., & Zhang, S. (2007). Western equatorial Pacific productivity and carbonate dissolution over the last 550 kyr: Foraminiferal and nannofossil evidence from ODP hole 807A. *Marine Micropaleontology*, *64*(3-4), 121–140. https://doi.org/10.1016/j.marmicro.2007.03.003